

Modulation Excitation Spectroscopy (MES)

Urakawa, Atsushi; Ferri, Davide; Nuguid, Rob Jeremiah G.

DOI

[10.1007/978-3-031-07125-6_42](https://doi.org/10.1007/978-3-031-07125-6_42)

Publication date

2023

Document Version

Final published version

Published in

Springer Handbooks

Citation (APA)

Urakawa, A., Ferri, D., & Nuguid, R. J. G. (2023). Modulation Excitation Spectroscopy (MES). In *Springer Handbooks* (pp. 967-977). (Springer Handbooks). Springer. https://doi.org/10.1007/978-3-031-07125-6_42

Important note

To cite this publication, please use the final published version (if applicable). Please check the document version above.

Copyright

Other than for strictly personal use, it is not permitted to download, forward or distribute the text or part of it, without the consent of the author(s) and/or copyright holder(s), unless the work is under an open content license such as Creative Commons.

Takedown policy

Please contact us and provide details if you believe this document breaches copyrights. We will remove access to the work immediately and investigate your claim.

Green Open Access added to TU Delft Institutional Repository

'You share, we take care!' - Taverne project

<https://www.openaccess.nl/en/you-share-we-take-care>

Otherwise as indicated in the copyright section: the publisher is the copyright holder of this work and the author uses the Dutch legislation to make this work public.



Contents

42.1 Introduction	967
42.2 Modulation and Phase-Sensitive Detection	968
42.3 Use and Interpretation of Phase-Resolved Data	971
42.4 Summary and Outlook	975
References	975

Abstract

In spectroscopy and diffraction methods, the signatures of catalytically active sites are often submerged by the contribution of spectator species. In some cases, the signals may also superimpose with each other, hindering proper peak identification. Rationalizing a reaction pathway becomes very challenging, if not impossible, under these circumstances. Accordingly, the implementation of transient, dynamic methods such as modulation/modulated excitation spectroscopy (MES) can improve the analysis of these signals. In MES, the catalyst sample is subjected to periodic changes in the environment (e.g., reactant concentration) that stimulate the active species periodically while spectra or diffractograms are recorded with sufficient time resolution. Combined with phase-sensitive

detection (PSD) analysis, this approach selectively enhances the signals of the responsive (and possibly active) species and at the same time attenuates the contribution from the spectator and static species. Overall, this results in increased analytical capabilities irrespective of the type of spectroscopy or diffraction technique that is used for the experiment. In this chapter, we introduce the basic concepts of MES, discuss the theory of PSD, and provide general guidelines that are useful for whoever encounters PSD data for the first time.

Keywords

Modulated/modulation excitation spectroscopy · Phase-sensitive detection · In situ · Operando · Spectroscopy · Diffraction

42.1 Introduction

In recent years, operando spectroscopy contributed to shedding light on the “black box” enclosing the mechanism of catalytic processes [1]. Through our knowledge of light-matter interaction, we have gained access to the molecular events occurring on the catalyst surface that was not possible a few decades ago. As a result, the rational design of catalytic materials is starting to become more realistic than ever, and the possibility to perform it is increasingly in our hands. Despite its great successes, however, modern spectroscopy still faces a number of limitations when applied to heterogeneous catalysis research due to the inherent complexity of solid catalytic systems. The prevailing difficulties stem from the following:

1. Catalysis results from simultaneous and often superimposed chemical phenomena [2]. These include reactant adsorption, surface reaction, and product desorption. As a consequence, the arising spectral signal will be a

A. Urakawa (✉)
Catalysis Engineering, Department of Chemical Engineering, Delft University of Technology, Delft, The Netherlands
e-mail: A.Urakawa@tudelft.nl

D. Ferri
Energy and Environment Research Division, Paul Scherrer Institut, Villigen, Switzerland
e-mail: davide.ferri@psi.ch

R. J. G. Nuguid
Energy and Environment Research Division, Paul Scherrer Institut, Villigen, Switzerland

École polytechnique fédérale de Lausanne (EPFL), Institute for Chemical Sciences and Engineering, Lausanne, Switzerland
e-mail: rob.nuguid@psi.ch

convolution of all of these processes. In some cases, one of the processes, thus its spectral features, will predominate over the others in a steady-state process. Furthermore, the spectroscopic signatures of different chemical species may have similar energy values and, in practice, appear as overlapping signals. For instance, Lewis-bound NH_3 , water, and nitrate species possess vibrational signature in the infrared (IR) spectrum at around 1620 cm^{-1} . The resulting observed peak is then the result of the overlap of the signals of these three species, with no straightforward way of deconvolution [3].

2. In commercial catalyst formulations, the active phase is present in a much lower concentration in comparison with the other catalyst components (e.g., support, promoter, and binder) in order to maximize the atom efficiency of the active phase, which is usually more expensive and not Earth-abundant. Conventional spectral features are therefore dominated by the signal originating from species coordinated to the support, while the active phase, which is the catalytically relevant component, can only contribute weakly because of its low concentration and the occurring turnover. In addition, the active phase itself can be further divided into catalytically relevant and spectator/unresponsive species. Normally, the spectator species predominate in number, and it remains a challenge to extract the signal contribution from the real species responsible for the activity [4].
3. Reactive intermediates are short-lived species owing to their thermodynamic instability. In rare instances, intermediate species are sufficiently stable that they can be isolated and characterized extensively. This is especially true for some organic reactions [5, 6], but it is not the norm for inorganic reactions and those that occur via a radical mechanism. The transient presence of intermediates in the reaction is further complicated by the fact that, compared to the reactants and products, only a very small fraction of the intermediates is present at any given time and thus will most likely be obscured by the signal contributed by the reactants and products.

Difference spectroscopy may partially solve the problem of separating the signal of the active phase from that of the support [7], but it fails to address the other issues. Chemometric methods can be employed to resolve complex envelopes of superimposed signals and are increasingly gaining popularity, but they normally require large datasets and computing power. Alternatively, a different experimental approach may be implemented. First described in a seminal work more than two decades ago [8], modulated excitation spectroscopy (MES, as it is also often called, modulation excitation spectroscopy) holds the potential of addressing all of the aforementioned difficulties.

42.2 Modulation and Phase-Sensitive Detection

Selective and sensitive detection of signals containing relevant information on catalytic reactions, such as catalytic active site/material and active chemical species, is of great challenge as described above in the limitations of general spectroscopic methods. MES is a transient response technique. It makes use of periodic perturbation of a reaction system with external parameter(s) called stimulus (or stimulation) [2, 8]. The stimulus is chosen in a way that the population of what we wish to monitor, e.g., the active catalyst structure or active chemical species, is affected most exclusively by the perturbation. Through the exclusive disturbance of particular species/structure and their subsequent detection, one can add *selectivity* to the detection. In principle, there is no limitation on the types of stimulus, and there are many examples such as fluid (gas/liquid) concentration [9, 10], temperature [11], electric field [12], light flux [13], and X-ray energy [14]. One can choose the most appropriate one depending on what one wishes to see and also on experimental convenience and restrictions. By far the most common stimulus type is fluid concentration, because the extent of a chemical reaction and the concentrations of active structure/species can be more easily modulated using a concentration stimulus [15].

The experimental protocol and data processing procedures are shown in Fig. 42.1. Let us assume that we use a periodic sinusoidal perturbation of a catalytic system by an external parameter as the stimulus (e.g., reactant concentration, Fig. 42.1a). At the start of such periodic perturbation experiments, typically there is an initial period when the chemical system changes irreversibly to some extent and reaches a stably oscillating period where the mean value is constant (quasi steady state, Fig. 42.1a). It should be noted that there is always some noise in the signal and the effects of noise are more significant when the time resolution of our measurements is increased (i.e., fast spectral acquisition). Figure 42.1 shows the stimulus and signal responses with lines, but in a typical spectroscopic measurement, we record signal responses as a function of a range of energy. The signal intensity shown in Fig. 42.1 represents a response only at one energy point, while in practice, there are distinct signal responses at every energy point recorded in a set of spectra (e.g., if IR spectroscopy is used and the spectra are recorded in the range of $1000\text{--}4000\text{ cm}^{-1}$ at the spectral resolution of 1 cm^{-1} , there are 3001 signal intensity responses in the recorded time-resolved data). For simplicity, here only one signal response at one energy point is described.

The first data processing generally performed in MES is a simple averaging of the signal over the cycles into one period after reaching a so-called quasi steady state after the initial equilibration period (Fig. 42.1b). According to Poisson

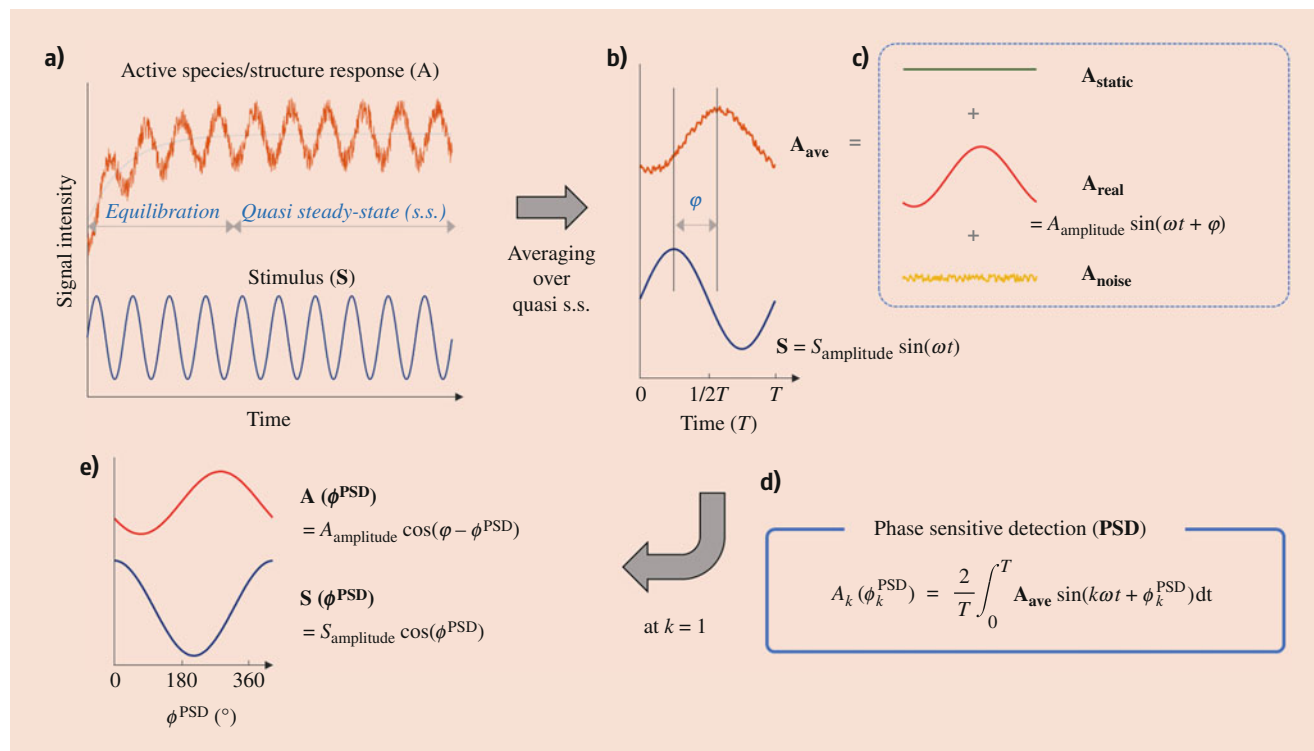


Fig. 42.1 (a) Sinusoidal stimulus of an external parameter and a representative response of active species/structures affected by the stimulus; (b) the one-period response obtained after averaging over the multiple modulation cycles after reaching quasi steady state; (c) the three signal elements consisting of the actual response (A_{ave}), namely

static signal (A_{static}), actual signal of interest (A_{real}), and noise (A_{noise}); (d) the mathematical engine of MES, phase-sensitive detection (PSD); and (e) the phase-domain response after PSD at the fundamental stimulus frequency demodulation ($k = 1$)

statistics, this reduces the data size and improves sensitivity as well as the signal-to-noise ratio by about \sqrt{N} . (N is the number of averaged cycles.) Actively responding species mainly respond at the same frequency as that of the stimulus, and the signal intensity oscillates in a sinusoidal manner but with some delay (ϕ) with respect to the stimulus (Fig. 42.1b). The magnitude of the delay is dependent on the kinetics of the underlying physicochemical processes (e.g., sorption, reaction, convection, and diffusion) and consequently the delay changes with the modulation frequency of the stimulus (ω). In other words, the frequency of the stimulus affects the magnitude of the delay, and kinetic studies can be performed by varying the stimulus frequency.

One can study the averaged response and its delay (Fig. 42.1b) to understand catalytic processes. However, the relative intensity of the signal actively changing in response to the stimulus is often extremely small and can be even at the level of noise. One can improve the signal-to-noise ratio by increasing the number of cycles (N), but this increases the burden in the experiments and data processing. In principle, the averaged signal (A_{ave}) consists of three signal elements (Fig. 42.1c): (i) static signal (A_{static}), (ii) actual signal of interest (A_{real}), and (iii) noise (A_{noise}). A_{static} may arise from catalyst support material, solvent, and inactive spectator

species, often dominating the detected signal. They are all important for the reaction one way or the other, but to understand the catalytic reactions, their dominant signal intensity should be reduced or eliminated completely. A_{real} is obviously the one we wish to extract to understand its chemical origin. A_{noise} is always present for any detection method, and typically it contains high-frequency elements with respect to the stimulus frequency. What we wish to do is to extract only A_{real} out of A_{ave} , and this is exactly what is done in MES by its mathematical processing, called phase-sensitive detection (PSD, Fig. 42.1d) [8].

PSD is the mathematical treatment often implemented in the hardware in signal processing such as lock-in amplifiers. On the other hand, the lock-in (i.e., extracting the signal at the same frequency as that of the stimulus, $k = 1$ in Fig. 42.1d) is performed numerically in MES, and this has major advantages over the hardware lock-in due to the richer information contained (i.e., less oversimplification of the data). What PSD does mathematically is presented by the equation in Fig. 42.1d. In a nutshell, the averaged signal (A_{ave}) is multiplied by another sine function at the frequency of $k\omega$. The sine function also contains a new variable ϕ_k^{PSD} which is called phase angle. Generally, the multiplied sine function has the fundamental frequency of the stimulus (ω), meaning

that $k = 1$ (if $k = 1$, k is often not written). The thus obtained response is integrated over the period (T) and then normalized by multiplying with $2/T$ (Fig. 42.1d). Interestingly, the resulting response after PSD is not a function of time any longer but of ϕ^{PSD} (Fig. 42.1e). PSD is also called demodulation, and k is sometimes called the demodulation index.

Let us evaluate what PSD does more closely. Regarding the stimulus, $S_{\text{amplitude}} \sin(\omega t)$ is transformed by PSD to a cosine function of the same amplitude ($S_{\text{amplitude}} \cos(\phi^{\text{PSD}})$) where the domain changes from time (t) to phase angle (ϕ^{PSD}). For the actively responding signal, the domain also changes and $A_{\text{amplitude}} \cos(\varphi - \phi^{\text{PSD}})$ is obtained after PSD. This phase-domain signal is a very similar sinusoidal function containing the delay term (φ) with the same amplitude as that of the signal we wish to extract (A_{real}) which is $A_{\text{amplitude}} \sin(\omega t + \varphi)$. Most importantly, in the phase domain, the static signal (A_{static}) is completely vanished and so is the noise (A_{noise}). Precisely, only the noise signal varying at the same frequency as $k\omega$ will appear in the phase domain, but this is negligible because high-frequency noise is generally dominating. Hence, what we can achieve with MES and especially by its mathematical engine PSD is that we can add *selectivity* to the measurement and boost its detection *sensitivity* by removing the static signals and reducing the noise while retaining the key information of interest. After PSD and the initial averaging process (Fig. 42.1b), in MES, one can often achieve 2–3 orders of magnitude improvement in signal-to-noise. This drastic improvement in the sensitivity is extremely useful or even necessary to study the weak and transiently present signals in catalytic reactions.

The mathematical expression for the active sites/species ($A_{\text{amplitude}} \cos(\varphi - \phi^{\text{PSD}})$, Fig. 42.1e), shows that the amplitude of the response ($A_{\text{amplitude}}$) is at its maximum when $\varphi - \phi^{\text{PSD}} = 0$, i.e., ϕ^{PSD} is equal to φ , which is called the “in-phase” condition. This “in-phase” condition has interesting and useful implications. From the phase-domain response, one can easily check when (at which phase angle) the signal becomes maximum by varying ϕ^{PSD} , and this value is directly related to the delay of the active species/structure. If we have multiple species and thus multiple bands in the time-resolved spectra with different kinetic responses, these bands will show maximum value in the phase domain at different ϕ^{PSD} . By converting in-phase ϕ^{PSD} to φ for different bands (e.g., different chemical species/structures), one can understand what is happening first and gain insights into transformation pathways. This analysis is called in-phase angle analysis [2, 16].

So far, a sinusoidal shape of stimulus has been assumed. In practice, this shape is often not the most convenient one to generate and, instead, a square-wave shaped stimulus is often used because such shapes can be more easily generated, for example, by valve switching for concentration modulation and by light on-off or by means of a chopper for light flux

modulation. One may wonder about the influence of the stimulus shape on the data analysis procedure and on the quantitative nature of such analysis. More precisely, the meaning of the amplitudes and delays of phase-domain signals when a square-wave stimulus is used can be questioned, compared to the case of the unaltered amplitude of the active species/structure signals after PSD when a sinusoidal stimulus is used (Fig. 42.1). Within the linear response approximation, the analysis procedure has been well established and shows even advantages of a square-wave stimulus compared to a sine-wave one [2, 17]. Mathematically, A square-wave (SW(t)) with an amplitude of A_{SW} can be written as the sum of odd-frequency sine functions with their amplitude scaled by the factor of $4/\pi$ and with more reducing amplitudes at higher frequencies.

$$\begin{aligned} \text{SW}(t) &= \frac{4}{\pi} A_{\text{SW}} \left(\sin \omega t + \frac{\sin 3\omega t}{3} + \frac{\sin 5\omega t}{5} + \dots \right) \\ &= \frac{4}{\pi} A_{\text{SW}} \sum_{n=1}^{\infty} \frac{\sin [(2n-1)\omega t]}{2n-1} \end{aligned} \quad (42.1)$$

Clearly, a square-wave contains the sine wave of the fundamental frequency besides all other sine waves of odd frequencies. In other words, with a square-wave stimulus, the system is perturbed not only by the fundamental frequency (ω) but also by the many higher frequencies (odd-frequency harmonics: 3ω , 5ω , 7ω , ...). The beauty of PSD is that by changing the demodulation index k in the PSD equation (Fig. 42.1d), we can selectively extract the response varying at $k\omega$ frequency, which can also be performed conveniently by Fourier transform [18]. It has been shown that the signal delay φ_k (in the phase domain, it is also called phase delay) obtained by the high-frequency demodulation (PSD with $k > 1$) is identical to that obtained with the MES experiment at the higher stimulus frequency as the fundamental frequency (e.g., MES experiment at $(2n-1)\omega$, n defined in Eq. 42.1). The same also holds for the response amplitude, but to convert the amplitude to a comparable scale, one needs to multiply the demodulated signal amplitude by $2n-1$ (Eq. 42.1) after high-frequency demodulation since the amplitudes of the higher frequency terms are smaller by $2n-1$ (Eq. 42.1). Importantly, this means that one square-wave stimulus experiment is equivalent to multiple sine-wave stimulus experiments, facilitating to understand the kinetic responses of the amplitude and delay of active signals. It should be remembered that this is precise and exact only when the responses are linear. In practice, one can obtain a more linear response by reducing the stimulus amplitude [17]. In this case, however, the amplitude of the higher frequency terms is also reduced, and the signal-to-noise ratio may not be high enough for reliable analysis.

42.3 Use and Interpretation of Phase-Resolved Data

The increasing number of reports on the use of MES and PSD to elucidate mechanisms of catalyzed reactions calls for an introduction into the use, analysis, and utility of the phase-resolved data. In order to keep the discussion broad enough, we consider two general signals close to each other (Fig. 42.2a). The abscissa is generic and could be mute, because the idea is to discuss any type of spectroscopy and diffraction experiment performed under the paradigm of the MES methodology. Moreover, it is clear from the PSD equation (Fig. 42.1d) that the formula is valid irrespective of the method that is used to interrogate the sample. This is

demonstrated by the increasing variety of analytical methods that have been coupled to the modulation approach in recent years (ATR-IR, DRIFTS, PM-IRRAS, Raman, XAS, XRD, XES, HEROS, and PDF) [15]. For the sake of clarity, we will refer to the spectra as the data in Fig. 42.2a–d.

Figure 42.2a, e represents a common graph that is encountered in most works making use of MES and PSD: time-resolved spectra (Fig. 42.2a) are presented together with their corresponding phase-resolved data (Fig. 42.2e) obtained at the fundamental demodulation frequency $k = 1$. In Fig. 42.2e, only half of the phase-resolved data upon PSD is presented. The other half of the data is a mirror image of these ones, as it follows from the sinusoidal phase angular dependence of signals. While the information delivered by

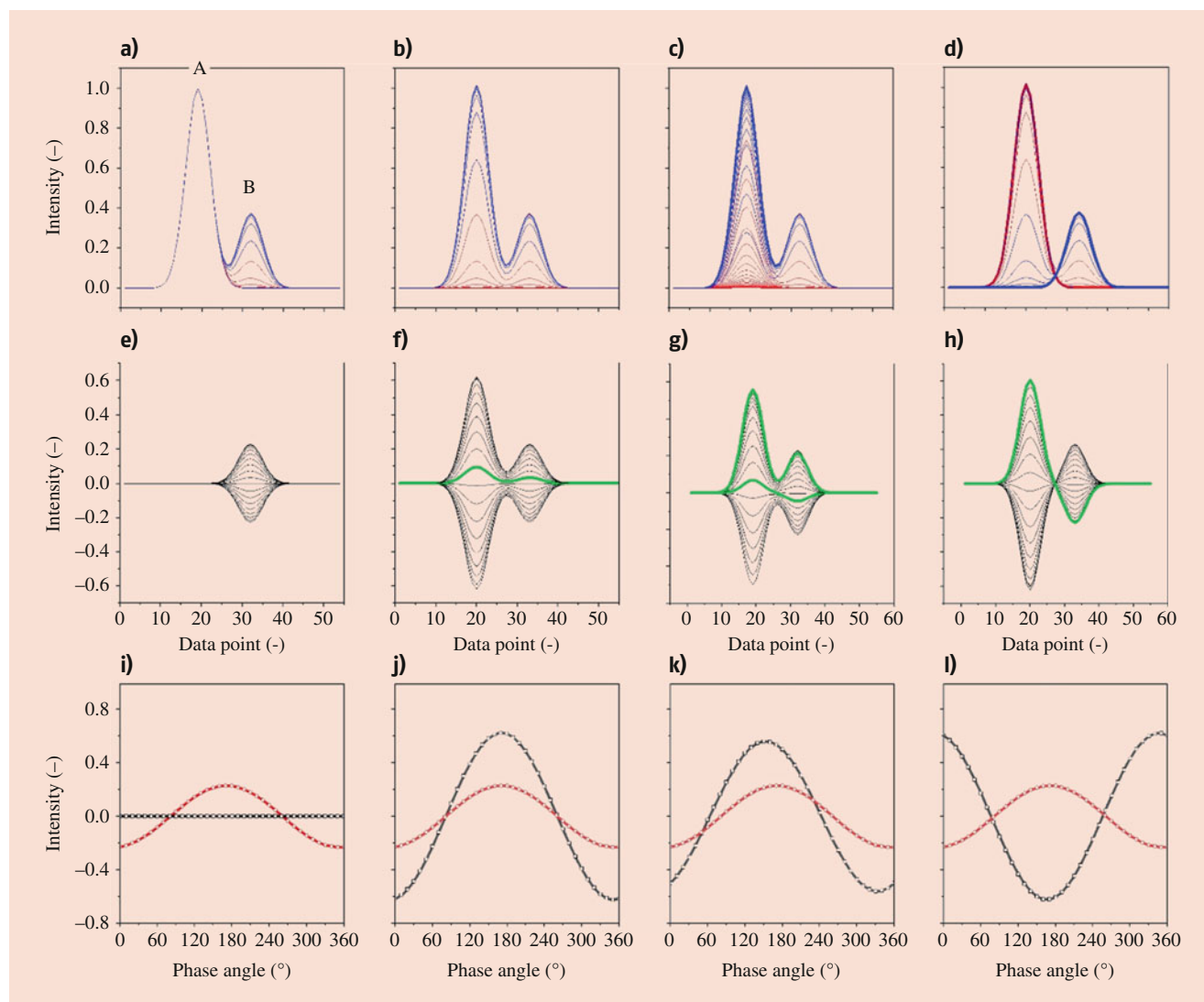


Fig. 42.2 (a–d) Simulated data sets of two generic signals A and B in modulated excitation experiments in which (a) A does not vary, (b) A and B vary with identical kinetics, (c) A is retarded compared to B, and (d) A is present when B is absent (i.e., opposite kinetics). (e–h) Corresponding phase-resolved data obtained at the fundamental

frequency of stimulus ($k = 1$). Only half of the full set of phase-resolved data is shown for simplicity. Green data are used to guide the eye and show relevant traces. (i–l) Phase angular dependence of A and B at the maximum peak position. Red data in (a–d) represents the first half-period, blue data the second half-period

comparison of Fig. 42.2a, e is inherently sufficient to claim that the signals appearing in the phase-resolved data belong to species responding to the external stimulus, there are a number of further actions that can be taken to analyze the phase-resolved data and take full advantage of MES.

Let us discuss the appearance of the phase-resolved data. Several sub-cases can be encountered that depend on how two signals behave with respect to each other along the time axis. We will discuss the following sub-cases: (a) one signal that we label as A remains unchanged, and the second (B) varies following a given kinetics of consumption and formation; (b) both signals vary following identical kinetics (synchronous); (c) both signals vary following different kinetics; and finally, (d), when A is present, B is not and vice versa (the signals vary with opposite phase; asynchronous). Figure 42.2a–d displays the sets of time-resolved spectra during one modulation period in which either B or both signals vary as indicated just above. Figure 42.3a–d presents the corresponding simulated temporal dependence of the two signals A and B in that modulation period. Ideally, the dataset of Fig. 42.2a–d is the result of averaging of e.g., n time-resolved spectra (in Fig. 42.3, $n = 40$) obtained in m modulation periods to a single modulation period, which we have shown above contributes to increase the signal-to-noise ratio of the measurement significantly [19–21].

Figure 42.2e–h show the corresponding phase-resolved dataset for each case obtained from application of the PSD equation using $k = 1$ and a half-period length $T/2$ (i.e., a half range of the whole ϕ^{PSD}). This PSD at $k = 1$ is very common for most characterization techniques enabling such measurements; however, for X-ray diffraction, it was demonstrated that active responses appear at $k = 2$ due to the fact that the detected intensity in XRD is the square of the scattered energy, leading to frequency doubling [22]. It should be noted that the maximum intensity of the signals in the phase-resolved data is typically scaled compared to the intensity of the changes in the time-resolved data (in the case of Fig. 42.2, the scaling factor is ca. 1.6; this scaling factor can be explained more precisely by considering that (i) the amplitude in the time domain is ca. 0.2 (Fig. 42.2a, b) and not ca. 0.4 since the amplitude change from the mean value is considered as in a sinusoidal wave); (ii) the amplitude obtained after PSD at $k = 1$ needs to be scaled by $4/\pi$ because of the square-wave stimulus and consequent scaling factor (Eq. 42.1); and (iii) $0.4/(0.2 \cdot 4/\pi)$ yields roughly 1.6 [23, 20].

In Fig. 42.2a, only signal B varies while signal A remains constant throughout the modulation period. The corresponding phase-resolved data shows only the contribution of signal B, because signal A does not change in intensity along the experiment and such signals are fully vanished by PSD (Fig. 42.1). The intensity of signal B changes from a maximum value to a minimum negative value following a sinusoidal function (Fig. 42.2i). The dataset of Fig. 42.2e is

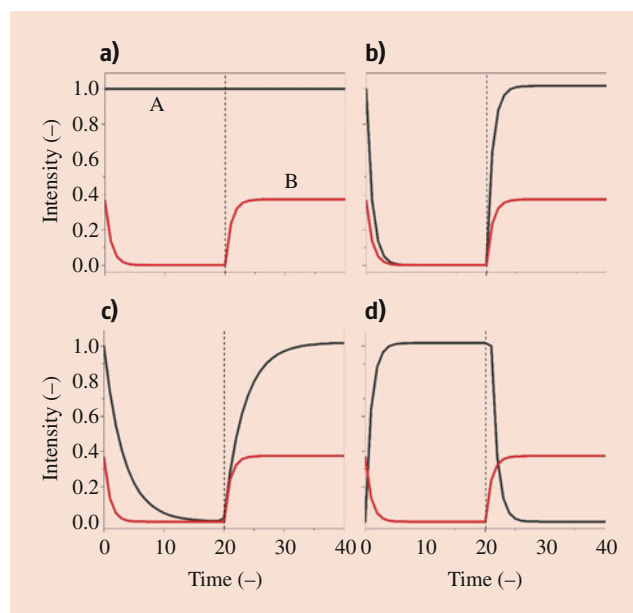


Fig. 42.3 Simulated temporal dependences of generic signals A and B. PSD of the corresponding time-resolved delivers the data shown in Fig. 42.2

composed of 18 spectra in the range of phase angles ϕ^{PSD} of $0\text{--}180^\circ$. In the $190\text{--}360^\circ$ range, the same set of spectra is obtained but of the opposite sign, following the sinusoidal phase angular dependence of signal intensity shown in Fig. 42.2i. This data set is shown with intervals of $\phi^{\text{PSD}} = 10^\circ$, but more precise intervals of 5, 2, or 1° can be obtained that might be required to better resolve kinetic behaviors of signals in phase-resolved data [24].

Consider then that also signal A varies during the modulation experiment and that the intensity of both signals exhibits the same kinetics of decay and evolution as shown in Fig. 42.3b. The two signals are set to exhibit different intensities. Figure 42.2f shows the phase-resolved spectra of this experiment. As in the previous case, the intensity of both signals varies along a sinusoidal function (Fig. 42.2j) and the two signals are in-phase as the maximum intensity reached by signal A corresponds to the maximum intensity obtained for signal B, but the two maxima do not correspond in absolute value. The phase angular dependence of the intensity of the two signals coincides (Fig. 42.2j); both signals cross the x -axis at the same points (phase angle, ϕ^{PSD}) and rise to the maximum and minimum values at the same points. This case is, for example, that very simple of an adsorbed species whose vibrational spectrum is composed of two signals A and B of different intensities: when the species appears in the experiment, both signals grow simultaneously when the species vanishes, both signals disappear with the same kinetics. This case could also be that of two species, one assigned to signal A and one to signal B, that display the same kinetic behavior.

A more complex case is that obtained when the two signals exhibit different kinetics but they still disappear/appear in the same half-period. Keeping the situation of two signals of different intensities, Fig. 42.2c shows very similar data to those of Fig. 42.2b. However, the kinetics of decay and growth clearly are not equal, implying that the phase-resolved data intersect. The phase-resolved data are also very similar to those shown in Fig. 42.2f. Here, the details are important. To explain, let us consider the phase angular dependence (Fig. 42.2k). Contrary to the previous case, the two sinusoids do not overlap; rather their maxima are shifted indicating a delay in the evolution of the two signals. This shift also reveals that, for example, at $\phi^{\text{PSD}} = 60^\circ$, signal A is absent in the phase-resolved spectrum, because its intensity is nil. Similarly, at $\phi^{\text{PSD}} = 80^\circ$, signal B intersects the x -axis and will not be present in the corresponding phase-resolved spectrum. This demonstrates that the spectra at these two ϕ^{PSD} values will display only the species corresponding to signal B and the species assigned to signal A, respectively. Therefore, spectra containing only the signal(s) of one species can be obtained by PSD and can be selected [2]. This analysis is the kinetic analysis of phase-resolved data. This may deliver the same results as the analysis of the time-resolved spectra as shown in Fig. 42.3 but could allow improving the differentiation of signals of different species that is sometimes not possible in the time-dependent dataset.

The other characteristic situation is shown in Fig. 42.2d, where the two signals are retarded by a half-period: when A is present, B is not, and vice versa in the subsequent half-period. This case may correspond to the situation when one species transforms into the other one, e.g., A transforms into B reversibly during the experiment. The corresponding phase-resolved data (Fig. 42.2h) always show lobes of the opposite sign. The phase angular dependence of the signals in Fig. 42.2l shows that signal A is maximum when signal B is minimum (and vice versa) and that both signals cross the x -axis at the same intersection points.

Clearly, the cases in Fig. 42.2a, c, and d represent two signals belonging to two different species. The above analysis suggests that rather than all phase-resolved data, a careful selection of the phase-resolved data can improve our knowledge about the behavior of the system.

While the analysis presented in Fig. 42.2 is relatively straightforward in the case of vibrational spectra [17, 25], it is particularly delicate in the case of X-ray absorption spectroscopy data. Given the nature of the experiment, there are a number of points within the sequence of transformations that can be performed on XAS data, from the raw near-edge data to the Fourier transformed data, that can provide different types of information. The raw XAS data can be treated by PSD as demonstrated in Refs. [19, 20, 26]. PSD at this point provides spectra in the whole energy range selected for the measurement that are very similar to difference spectra

(though with significantly enhanced signal-to-noise ratio). This allows the visualization of subtle changes in oxidation state by the absorbing element, even for low levels of the absorbing element, e.g., 0.3 wt% Rh/Al₂O₃, hence likely for very small aggregated entities of the active phase [19]. Comparison with a difference spectrum obtained from the metal foil and a corresponding spectrum of an oxidized phase of the element (for example, PdO in the case of Pd) can support qualitative identification of additional phases. This has been, for instance, the case for the presence of Pd-C species in modulation experiments consisting of alternate pulses of CO and NO on Pd/Al₂O₃ [19]. Large deviations of the phase-resolved spectra in the region starting 5 eV above the Pd K-edge ($E_0 = 24,350$ eV) from the Pd-PdO difference spectrum provided qualitative information on the formation of carbide species that were reflected in the quantitative analysis of the time-resolved EXAFS spectra, suggesting expansion of the Pd-Pd bond length in the CO pulse from 2.73 to ca. 2.77 Å. The PSD of the normalized raw data cancels the contribution of the edge jump that hampers identification of small changes around the edge energy and the whiteline as well as of the predominant phase. Continuing with the example of reduced Pd/Al₂O₃, the contribution of metallic Pd representing the bulk of Pd nano-particles after reduction in this material is cancelled by PSD.

For quantitative purposes, Chiarello et al. [23] showed that for XAS data, PSD can be carried out on the data in the k -space followed by or after Fourier transform. While the information contained in the PSD data should ideally be identical, demodulation in k -space followed by Fourier transform of the PSD data is preferable to visualize only the changes occurring on the radial distribution function. Hence, changes in the distances from neighboring atoms and in the coordination number relative to a specific coordination shell are made visible by PSD. Because PSD eliminates the contribution of species to the spectra that do not respond to the modulation stimulus, the PSD of the k -space data eliminates the contribution of the bulk phase that may dominate in the radial distribution function. This approach allowed the determination of small coordination number values from fitting the data after sequential PSD and Fourier transform, suggesting the growth of thin oxidic layers on metal particles. For example, on nano-particles of typical sizes of 2–6 nm, values for Pd-O and Pd-O-Pd were 2.0 ± 0.2 and 1.8 ± 0.6 , respectively, for Pd/Al₂O₃ [23]. On larger particles (>10 nm), where the contribution of the bulk to the XAS is even larger, an average Ru-O coordination number of 0.25 ± 0.09 , a bond distance of 1.945 ± 0.016 Å, and a pseudo-Debye-Waller factor of 0.0035 ± 0.0035 Å² were determined for a reduced Ru/Al₂O₃ catalyst subject to periodic oxidation-reduction indicating the presence of a very thin oxide layer [20]. On the contrary, the PSD data after Fourier transform contain also the information on the bulk

phases [25], which overlaps strongly with the changes induced by the modulation typically overwhelming them.

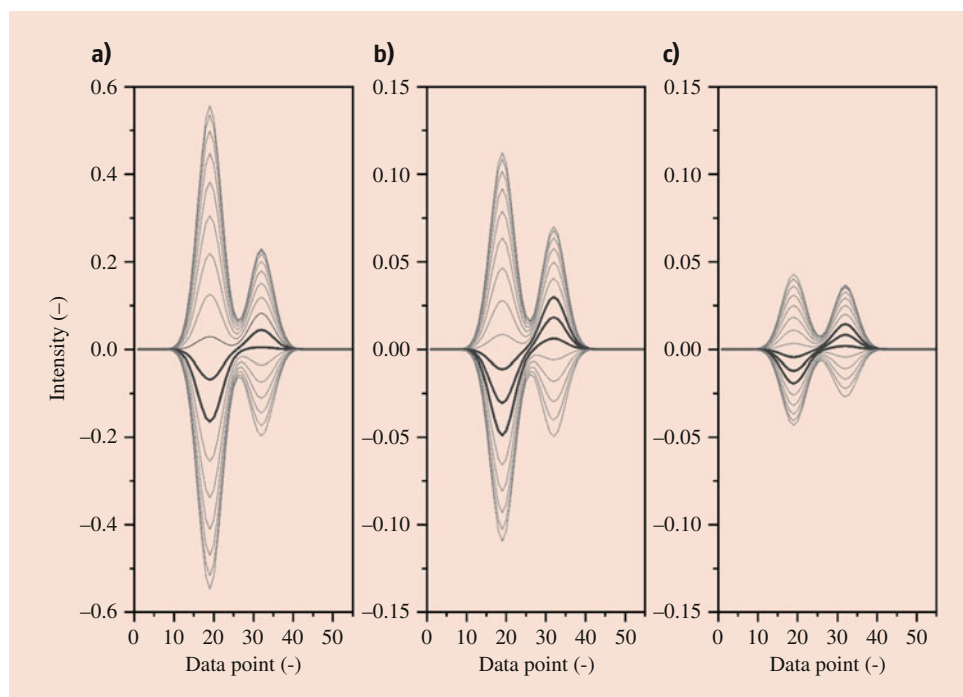
König et al. [24] have shown that the modulation-PSD approach provides sufficient sensitivity to detect Ru-S bonds in Al₂O₃-supported Ru that are believed to be located at the surface of the large Ru particles (10–30 nm) with a Ru-S coordination number of 0.07 ± 0.02 at $R = 2.299 \pm 0.012$. This analysis of enhanced precision was possible only upon the selection of suitable phase-resolved spectra among the obtained set, as we have described in Fig. 42.2. Given the surface nature of the heterogeneous catalytic processes, the studies using XAS combined with modulated excitation and PSD demonstrate that surface sensitivity can be bestowed on XAS through this experimental approach.

We believe that this is also the case for XRD, another typical bulk characterization method. High energy XRD modulation experiments on Pd supported on ceria-zirconia demonstrated the potential of XRD in determining the redox behavior of small metal nano-particles that are otherwise not resolved by XRD [21], especially because of the contribution of the background scattering. This is completely removed by the PSD thus allowing the observation of small diffraction peaks. Marchionni et al. [27, 28] showed that reoxidation of reduced Pd/Al₂O₃ occurs in two stages using high-energy XRD. The phase-resolved XRD data exhibited different degrees of combination of two features of different widths in the range of the (101) reflection of PdO ($2\theta = 32.5^\circ$). The kinetic analysis demonstrated above, upon adequate selection of the phase-resolved data, allowed to isolate the contribution

of an amorphous phase ($\phi^{\text{PSD}} = 210^\circ$), characterized by a very broad signal, from that of a more crystalline phase ($\phi^{\text{PSD}} = 70^\circ$), characterized by an overlapping sharp signal [27]. Alternate CO and O₂ pulses allowed demonstrating that Pt nano-particles in Pt/Al₂O₃ oscillate between fully reduced and an amorphous Pt-O layer [29]. The corresponding phase-resolved XRD data (belonging to the case shown in Fig. 42.2d) displayed sharp peaks in correspondence of Pt reflections and very broad features of the opposite sign in correspondence of the Pt oxide reflections.

While most phase-resolved data are typically obtained and shown at $k = 1$, further analysis can be performed upon demodulation using higher harmonics, typically $k = 3, 5$, etc. [17, 25, 27]. This additional analysis is useful to distinguish between species of different nature when this differentiation is ambiguous at $k = 1$. A detailed mathematical analysis is provided in Ref. [27] in combination with kinetic considerations. Figure 42.4 shows the same data as in Fig. 42.2c after PSD at $k = 1, 3$ and 5. The major effect of the use of higher harmonics on the sets of phase resolved data is to decrease the overall intensity, which is more significant at $k = 3$ (Fig. 42.4b) and attenuates above this value. This is the case because the contribution of higher harmonics to the approximation of a square-wave stimulus decreases with increasing k [2]. However, Fig. 42.4 also shows that the decrease in intensity with increasing k occurs faster for signal A, the A:B ratio decreasing in the order of $2.45 (k = 1) > 1.60 (3) > 1.17 (5)$. Hence, in this process, a simultaneous enhancement in the response of signals whose

Fig. 42.4 Sets of phase-resolved data are obtained from PSD of the time-resolved data of Fig. 42.2c using (a) $k = 1$ (identical to Fig. 42.2g), (b) 3, and (c) 5. Bold traces are used to guide the eye and to highlight data where the two signals A and B have the opposite sign. For simplicity, only half of the full set of phase-resolved data is shown



temporal dependence is faster is obtained relative to signals evolving more slowly. In the case considered here, the decreased A:B ratio with increasing k agrees with the temporal profiles of A and B signals in Fig. 42.3c, showing that signal B appears and disappears faster than signal A in both half-periods. It is also evident that with increasing k , it becomes easier to see differences between the kinetics of the two signals, as an increasing number of phase-resolved data exhibits signals of opposite sign with increasing k .

42.4 Summary and Outlook

Over the last few decades, advances in nano-material engineering and improvements in in situ and operando detection methodologies have significantly enhanced our understanding of catalytic materials and reaction mechanisms. At the same time, many studies have exemplified the dynamic nature of catalyst materials responding to reaction conditions (reactant/product concentration, pressure, and temperature), highlighting the necessity for operando studies to firmly establish structure vs. activity relationships towards rational design and optimization of next generation catalysts. These technological advances, however, are often not sufficient to sense active chemical species and catalytic active sites due to their low populations compared to other inactive or irrelevant chemical species and material structures. MES allows both adding detection selectivity towards what we wish to monitor (active sites/structures) and boosting sensitivity drastically through the averaging scheme and the subsequent mathematical treatment, PSD. There are numerous application examples demonstrating the power of MES in studying catalytic reaction mechanisms [15], and this approach is increasingly gaining popularity over the past decade due to its necessity as well as its versatile character to combine with any analytical methods.

The important aspect which is not covered in this chapter is the cell design to perform MES experiments. As described above, various stimulus types can be used and, among them, concentration modulation is the most common type of experiment. It is very important to design spectroscopic cells so that one can perform relevant studies (i.e., operando, with simultaneous reactivity measurement) and exert a stimulus with a desired shape (e.g., sinusoidal or square wave). Flow-through cells are commonly used for concentration modulation, and it is of critical importance to characterize the flow and mixing behavior to precisely evaluate chemical information. For reaction kinetic analysis, it is mandatory to characterize in situ and operando cells in depth by understanding convection and diffusion, thus their nonideal behavior as reactors and their influences on the signal responses [10, 30–33]. When a stimulus is created by using substrates of chemically identical nature such as isotopes [34, 35], it is possible to combine MES with detailed kinetic studies using

the scheme of steady-state isotopic transient kinetic analysis (SSITKA) [36] to elucidate molecular interactions, reaction mechanisms, and reaction kinetics.

It is also important to highlight one major challenge with MES on disentangling overlapping bands in the phase domain. In theory, from the in-phase angles, one can differentiate kinetics of the bands with a distinct chemical nature; however, this fails largely when bands overlap because they show mixed in-phase angles of the underlying bands. It is possible to enhance the kinetic resolution of the bands with different chemical origins by making use of high-frequency demodulation (Fig. 42.4); however, it is not straightforward to obtain chemically and kinetically pure spectra by MES. To solve this problem, one can use multivariate spectral analysis such as multivariate curve resolution (MCR) [37, 38]. Recently, combining the advantages of MES for sensitivity enhancement and disentangling power of multivariate spectral analysis has been demonstrated [39, 40]. Further applications of these new methodologies, their theoretical development, as well as more insightful and detailed MES studies are expected and are necessary to maximally make use of these powerful methodologies for mechanistic and kinetic studies of catalytic systems.

References

1. Weckhuysen, B.M.: In Situ Spectroscopy of Catalysts, vol. 36. American Scientific Publishers (2004)
2. Urakawa, A., Bürgi, T., Baiker, A.: Sensitivity enhancement and dynamic behavior analysis by modulation excitation spectroscopy: principle and application in heterogeneous catalysis. *Chem. Eng. Sci.* **63**, 4902–4909 (2008)
3. Rasmussen, S.B., Portela, R., Bazin, P., Avila, P., Banares, M.A., Daturi, M.: Transientoperandostudy on the $\text{NH}_3/\text{NH}_4^+$ interplay in V-SCR monolithic catalysts. *Appl Catal B.* **224**, 109–115 (2018)
4. Kopelent, R., van Bokhoven, J.A., Szlachetko, J., Edebeli, J., Paun, C., Nachttegaal, M., Safonova, O.V.: Catalytically active and spectator Ce^{3+} in Ceria-supported metal catalysts. *Angew. Chem. Int. Ed.* **54**, 8728–8731 (2015)
5. Crandall, J.K., Conover, W.W., Komin, J.B., Machleder, W.H.: Allene epoxidation. Isolation of reactive intermediates from hindered allenes. *J. Org. Chem.* **39**, 1723–1729 (1974)
6. Proulx, G., Bergman, R.G.: Synthesis, structures, and kinetics and mechanism of decomposition of terminal metal azide complexes: isolated intermediates in the formation of imidometal complexes from organic azides. *Organometallics.* **15**, 684–692 (1996)
7. Grdadolnik, J.: Infrared difference spectroscopy Part I. Interpretation of the difference spectrum. *Vibr Spectrosc.* **31**, 279–288 (2003)
8. Baurecht, D., Fringeli, U.P.: Quantitative modulated excitation Fourier transform infrared spectroscopy. *Rev Sci Instr.* **72**, 3782–3792 (2001)
9. Bürgi, T., Baiker, A.: In situ infrared spectroscopy of catalytic solid-liquid interfaces using phase-sensitive detection: enantioselective hydrogenation of a pyrone over Pd/TiO₂. *J. Phys. Chem. B.* **106**(41), 10649–10658 (2002). <https://doi.org/10.1021/jp0255987>
10. Urakawa, A., Wirz, R., Bürgi, T., Baiker, A.: ATR-IR flow-through cell for concentration modulation excitation spectroscopy: diffusion

- experiments and simulations. *J. Phys. Chem. B.* **107**(47), 13061–13068 (2003)
11. Caliendo, R., Chernyshov, D., Emerich, H., Milanesio, M., Palin, L., Urakawa, A., van Beek, W., Viterbo, D.: Patterson selectivity by modulation-enhanced diffraction. *J. Appl. Crystallogr.* **45**, 458–470 (2012). <https://doi.org/10.1107/s0021889812011569>
 12. Schwarzott, M., Lasch, P., Baurecht, D., Naumann, D., Fringeli, U.P.: Electric field-induced changes in lipids investigated by modulated excitation FTIR spectroscopy. *Biophys. J.* **86**(1), 285–295 (2004). [https://doi.org/10.1016/s0006-3495\(04\)74104-1](https://doi.org/10.1016/s0006-3495(04)74104-1)
 13. Borges Ordoño, M., Yasumura, S., Glatzel, P., Urakawa, A.: Synergistic interplay of Zn and Rh-Cr promoters on Ga₂O₃ based photocatalysts for water splitting. *Phys. Chem. Chem. Phys.* **20**(36), 23515–23521 (2018). <https://doi.org/10.1039/c8cp03987a>
 14. van Beek, W., Emerich, H., Urakawa, A., Palin, L., Milanesio, M., Caliendo, R., Viterbo, D., Chernyshov, D.: Untangling diffraction intensity: modulation enhanced diffraction on ZrO₂ powder. *J. Appl. Crystallogr.* **45**, 738–747 (2012). <https://doi.org/10.1107/s0021889812018109>
 15. Müller, P., Hermans, I.: Applications of modulation excitation spectroscopy in heterogeneous catalysis. *Ind. Eng. Chem. Res.* **56**, 1123–1136 (2017)
 16. Urakawa, A., Van Beek, W., Monrabal-Capilla, M., Galán-Mascarós, J.R., Palin, L., Milanesio, M.: Combined, modulation enhanced X-ray powder diffraction and Raman spectroscopic study of structural transitions in the spin crossover material [Fe(Htrz)₂(trz)] (BF₄). *J. Phys. Chem. C.* **115**(4), 1323–1329 (2011). <https://doi.org/10.1021/jp107206n>
 17. Urakawa, A., Bürgi, T., Baiker, A.: Kinetic analysis using square-wave stimulation in modulation excitation spectroscopy: mixing property of a flow-through PM-IRRAS cell. *Chem. Phys.* **324**, 653–658 (2006)
 18. Srinivasan, P.D., Patil, B.S., Zhu, H.D., Bravo-Suarez, J.J.: Application of modulation excitation-phase sensitive detection-DRIFTS for in situ/operando characterization of heterogeneous catalysts. *React. Chem. Eng.* **4**(5), 862–883 (2019). <https://doi.org/10.1039/c9re00011a>
 19. Ferri, D., Matam, S.K., Wirz, R., Eyssler, A., Korsak, O., Hug, P., Weidenkaff, A., Newton, M.A.: First steps in combining modulation excitation spectroscopy with synchronous dispersive EXAFS/DRIFTS/mass spectrometry for in situ time resolved study of heterogeneous catalysts. *PCCP.* **12**, 5634 (2010)
 20. König, C.F.J., van Bokhoven, J.A., Schildhauer, T.J., Nachttegaal, M.: Quantitative analysis of modulated excitation X-ray absorption spectra: enhanced precision of EXAFS fitting. *J. Phys. Chem. C.* **116**, 19857–19866 (2012)
 21. Ferri, D., Newton, M.A., Di Michiel, M., Chiarello, G.L., Yoon, S., Lu, Y., Andrieux, J.: Revealing the dynamic structure of complex solid catalysts using modulated excitation X-ray diffraction. *Angew. Chem. Int. Ed.* **53**, 8890–8894 (2014)
 22. Chernyshov, D., van Beek, W., Emerich, H., Milanesio, M., Urakawa, A., Viterbo, D., Palin, L., Caliendo, R.: Kinematic diffraction on a structure with periodically varying scattering function. *Acta Cryst.* **A67**, 327–335 (2011)
 23. Chiarello, G.L., Ferri, D.: Modulated excitation extended X-ray absorption fine structure spectroscopy. *PCCP.* **17**, 10579 (2015)
 24. König, C.F.J., Schildhauer, T.J., Nachttegaal, M.: Methane synthesis and sulfur removal over a Ru catalyst probed in situ with high sensitivity X-ray absorption spectroscopy. *J. Catal.* **305**, 92–100 (2013)
 25. Marchionni, V., Newton, M.A., Kambolis, A., Matam, S.K., Weidenkaff, A., Ferri, D.: A modulated excitation ED-EXAFS/DRIFTS study of hydrothermal ageing of Rh/Al₂O₃. *Catal. Today.* **229**, 80–87 (2014)
 26. Ferri, D., Newton, M.A., Nachttegaal, M.: Modulation excitation X-ray absorption spectroscopy to probe surface species on heterogeneous catalysts. *Top. Catal.* **54**, 1070–1078 (2011)
 27. Marchionni, V., Ferri, D., Kröcher, O., Wokaun, A.: Increasing the sensitivity to short-lived species in a modulated excitation experiment. *Anal. Chem.* **89**, 5801–5809 (2017)
 28. Marchionni, V., Nachttegaal, M., Ferri, D.: Influence of CO on dry CH₄ oxidation on Pd/Al₂O₃ by operando spectroscopy: a multi-technique modulated excitation study. *ACS Catal.* **10**, 4791–4804 (2020)
 29. Marchionni, V., Kambolis, A., Nachttegaal, M., Kröcher, O., Ferri, D.: High energy X-ray diffraction and IR spectroscopy of Pt/Al₂O₃ during CO oxidation in a novel catalytic reactor cell. *Catal. Struct. React.* **3**, 71–78 (2016)
 30. Meier, D.M., Urakawa, A., Baiker, A.: Polarization-modulation infrared reflection-absorption spectroscopy affording time-resolved simultaneous detection of surface and liquid phase species at catalytic solid-liquid interfaces. *Analyst.* **134**(9), 1779–1780 (2009). <https://doi.org/10.1039/b911151d>
 31. Urakawa, A., Bürgi, T., Schläpfer, H.-P., Baiker, A.: Simultaneous in situ monitoring of surface and gas species and surface properties by Modulation Excitation PM-IRRAS: CO oxidation over Pt film. *J. Chem. Phys.* **124**, 054717 (2006)
 32. Bieri, M., Bürgi, T.: Probing enantiospecific interactions between proline and an L-glutathione self-assembled monolayer by modulation excitation ATR-IR spectroscopy. *J. Phys. Chem. B.* **109**(20), 10243–10250 (2005). <https://doi.org/10.1021/jp050197n>
 33. Patil, B.S., Srinivasan, P.D., Atchison, E., Zhu, H.D., Bravo-Suarez, J.J.: Design, modelling, and application of a low void-volume in situ diffuse reflectance spectroscopic reaction cell for transient catalytic studies. *React. Chem. Eng.* **4**(4), 667–678 (2019). <https://doi.org/10.1039/c8re00302e>
 34. Maeda, N., Meemken, F., Baiker, A.: Insight into the mechanism of the preferential oxidation of carbon monoxide by using isotope-modulated excitation IR spectroscopy. *ChemCatChem.* **5**(8), 2199–2202 (2013). <https://doi.org/10.1002/cctc.201300172>
 35. Pavelko, R.G., Choi, J.-K., Urakawa, A., Yuasa, M., Kida, T., Shimano, K.: H₂O/D₂O exchange on SnO₂ materials in the presence of CO: operando spectroscopic and electric resistance measurements. *J. Phys. Chem. C.* **118**(5), 2554–2563 (2014). <https://doi.org/10.1021/jp4108766>
 36. Ledesma, C., Yang, J., Chen, D., Holmen, A.: Recent approaches in mechanistic and kinetic studies of catalytic reactions using SSITKA technique. *ACS Catal.* **4**(12), 4527–4547 (2014). <https://doi.org/10.1021/cs501264f>
 37. Voronov, A., Urakawa, A., van Beek, W., Tsakoumis, N.E., Emerich, H., Rønning, M.: Multivariate curve resolution applied to *in situ* X-ray absorption spectroscopy data: an efficient tool for data processing and analysis. *Anal. Chim. Acta.* **840**, 20–27 (2014). <https://doi.org/10.1016/j.aca.2014.06.050>
 38. Urakawa, A.: Trends and advances in operando methodology. *Curr. Opin. Chem. Eng.* **12**, 31–36 (2016). <https://doi.org/10.1016/j.coche.2016.02.002>
 39. Alcaraz, M.R., Aguirre, A., Goicoechea, H.C., Culzoni, M.J., Collins, S.E.: Resolution of intermediate surface species by combining modulated infrared spectroscopy and chemometrics. *Anal. Chim. Acta.* **1049**, 38–46 (2019). <https://doi.org/10.1016/j.aca.2018.10.052>
 40. Witzke, M.E., Almithn, A., Coonrod, C.L., Triezenberg, M.D., Hibbitts, D.D., Flaherty, D.W.: In situ methods for identifying reactive surface intermediates during hydrogenolysis reactions: C–O bond cleavage on nanoparticles of nickel and nickel phosphides. *J. Am. Chem. Soc.* **141**(42), 16671–16684 (2019). <https://doi.org/10.1021/jacs.9b06112>



Atsushi Urakawa is Professor of Catalysis Engineering at the Department of Chemical Engineering, Delft University of Technology (The Netherlands). His research team combines fundamental and applied approaches for catalysis research and focuses on the rational development of heterogeneous catalysts and processes aided by in situ and operando methodologies.



Rob Jeremiah G. Nuguid currently works at Linde GmbH (Germany). He obtained his PhD degree from École polytechnique fédérale de Lausanne and Paul Scherrer Institut (Switzerland), where he used time-resolved spectroscopy to uncover the mechanisms of catalytic reactions.



Davide Ferri received his PhD in chemistry at the ETH Zurich in 2002. He is currently head of the group for Applied Catalysis and Spectroscopy at the Paul Scherrer Institut (Switzerland). His interests span from environmental catalysts to liquid-phase catalyzed reactions and the development of in situ/operando experiments. He uses vibrational spectroscopies in combination with X-ray based methods.